Science Advances
AAAS

Supplementary Materials for

Ensemble-function relationships to dissect mechanisms of enzyme catalysis

Filip Yabukarski *et al.*

Corresponding author: Filip Yabukarski, fyabukarski@gmail.com; Daniel Herschlag, herschla@stanford.edu

Sci. Adv. **8**, eabn7738 (2022)
DOI: 10.1126/sciadv.abn7738

This PDF file includes:

Supplementary Text
Figs. S1 to S6
Tables S1 to S7
References

Supplementary text 1

Hydrogen bond length and energetics.

Proposals to explain enzyme catalysis have invoked a relationship between the hydrogen bond length and the hydrogen bond strength, with the shortest hydrogen bonds proposed to be the strongest (*91*–*94*). Such short hydrogen bonds are often also called "low barrier" hydrogen bonds and may result in the average position of the hydrogen atom is at the center between the two hydrogen bonding heavy atoms. Low-barrier hydrogen bond energetic proposals have been discussed extensively and are distinct from hydrogen bond effects addressed herein where hydrogen bond length and energetics arise from reduced polarization of the Y16 KSI hydrogen bond from disruption of the Y57/Y32 hydrogen bond network with Y16 (*46*, *50*, *52*, *91*, *95*–*98*).

Supplementary text 2

KSI oxyanion hole hydrogen bond length changes.

Because we expect and observe a shortening of the Y16 hydrogen bond with changes in hydrogen bond polarization, there must be some change in the oxyanion hole conformational state. However, for Y32F/Y57F the observed 0.1 Å change in the Y16 hydrogen bond length is small relative to the conformational motions of Y16 and the oxyanion (on the scale of 1 Å) and therefore not expected to significantly impact the ensemble (*23*). In addition, prior work has established coupling between hydrogen bonds such that shortening of the D103 hydrogen bond is expected to accompany Y16 lengthening, with an effect of 0.3 that of the primary Y16 effect (*50*, *99*). This effect is observed for the Y32F/Y57F (*50*) and Y57F mutants (**Figure S3** and **Table S5**); it is also small relative to overall conformational motions and there are no additional effects of the Y32F/Y57F and Y57F mutations on the conformational states of D103 (see **Figure S2**).

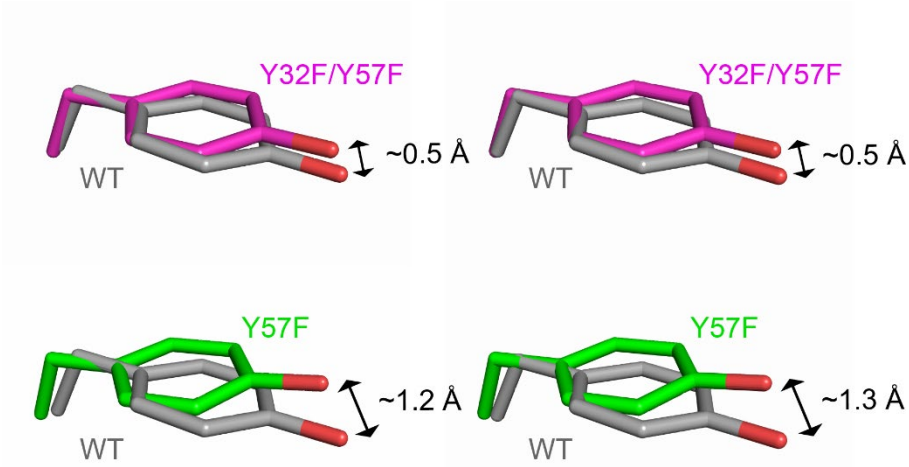

Figure S1. Comparison of the Y16 position in WT (PDB 3VSY, grey, (*35*)), Y32F/Y57F (PDB 1DMN, magenta, (*3*)), and Y57F (PDB 1DMM, green, (*3*)). The WT crystal structure contains two molecules (dimer) in the asymmetric unit: molecule A (comparison on the left) and molecule B (comparison on the right), while Y32F/Y57F and Y57F asymmetric unit contains a single KSI molecule (monomer) and the KSI dimer can be reproduced by applying crystallographic two-fold symmetry. The KSI molecules are aligned on the protein backbone (atoms N, CA, C, O, see Materials and Methods). See **Table S1** for RMSDs.

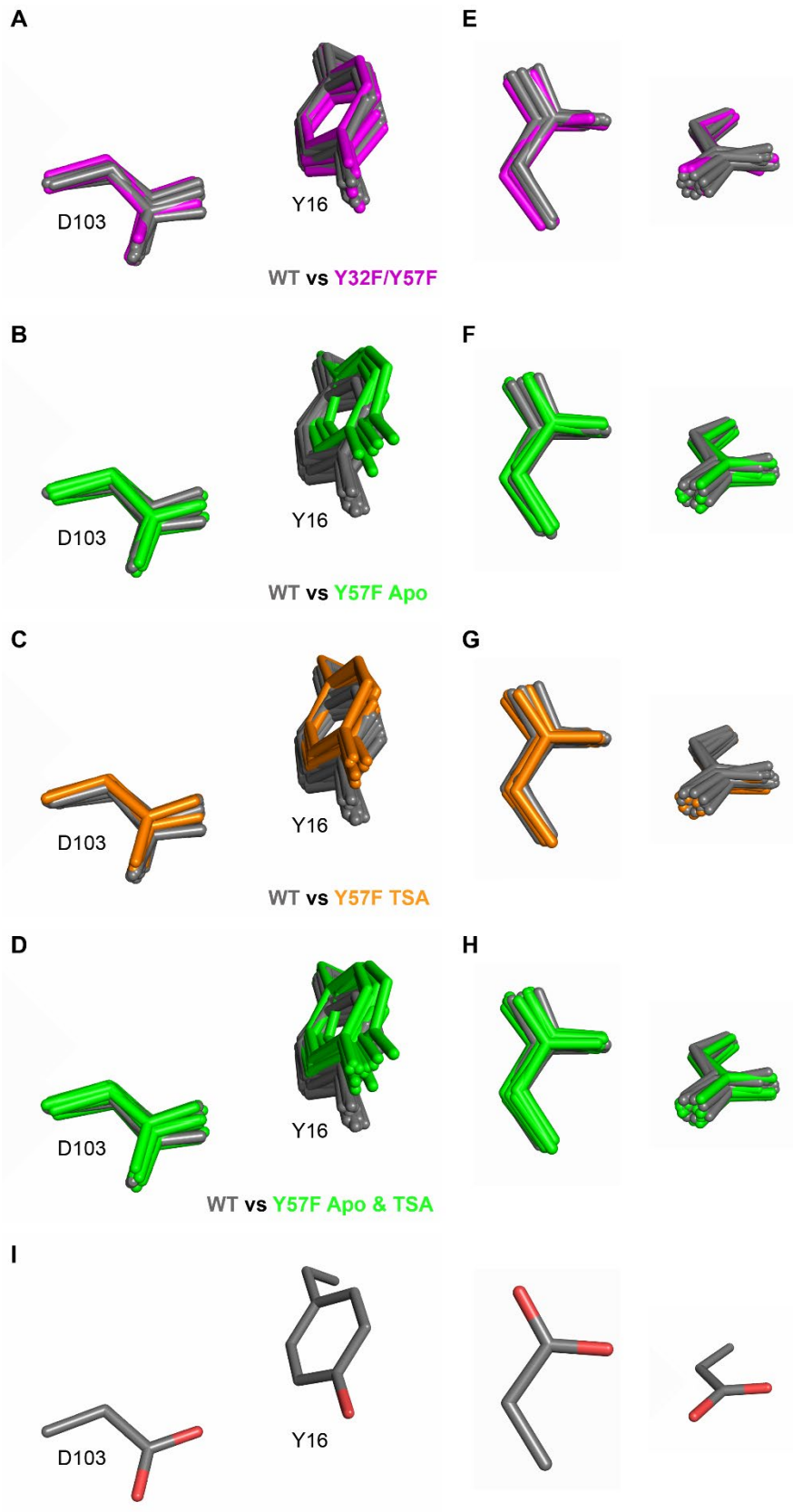

Figure S2. Comparison of WT and mutant oxyanion hole Y16 and D103 ensembles and multi-conformer models. Overlay of the WT ensemble (grey) with the multi-conformer models for (**A**) Y32F/Y57F (magenta), (**B**) Y57F apo, (**C**) Y57F TSA-bound (orange), and (**D**) Y57F apo and TSA-bound (green). For both WT and mutants, each KSI state is composed of the multi-conformer models for each monomer from the KSI dimer. Thus, the WT ensemble is composed of 2 multi-conformer models for each of the apo, GSA-bound, and TSA-bound states (*23*). For each mutant, each state is composed of two multi-conformer models. Thus the comparisons in (A-C) are between the WT ensemble and the two Y32F/Y57F apo multi-conformer models, the two Y57F apo multi-conformer models, and the two Y57F TSA-bound multi-conformer models, respectively. In (D) all four Y57F multi-conformer models (apo and TSA-bound) are compared with the WT ensemble. (**I**) Illustrates the orientation of Y16 and D103 in (A-D) but with the oxygen atoms colored in red. (**E-H**) The same comparisons as for (A-D) but now only shown D103 in two different orientations. The comparisons suggest no changes in the D103 ensembles in any of the mutants relative to WT.

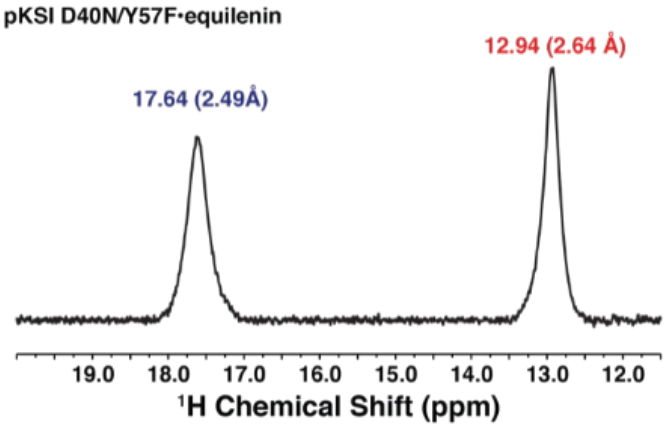

Figure S3. ^{1}H NMR spectrum for Y57F/D40N with bound TSA. The Y57F/D40N – transition state analog complex was prepared and data was collected as described in the Materials and Methods. D40N mutation was introduced to mimic the protonated general base and increase TSA affinity (*52*, *53*).

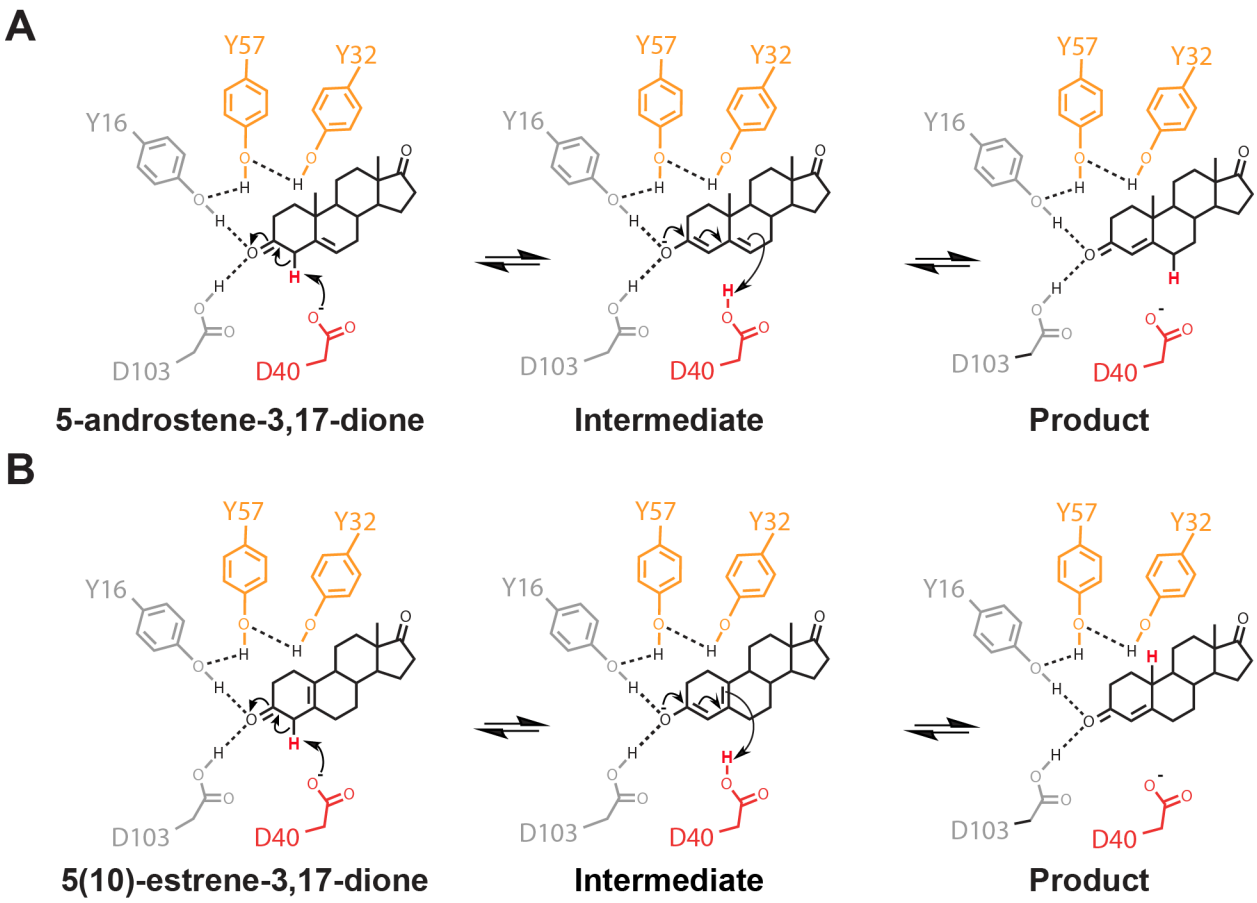

Figure S4. KSI reaction mechanism with the steroid substrates 5-androstene-3,17-dione (A) and 5(10)-estrene-3,17-dione (B). The shuffled proton is colored in red.

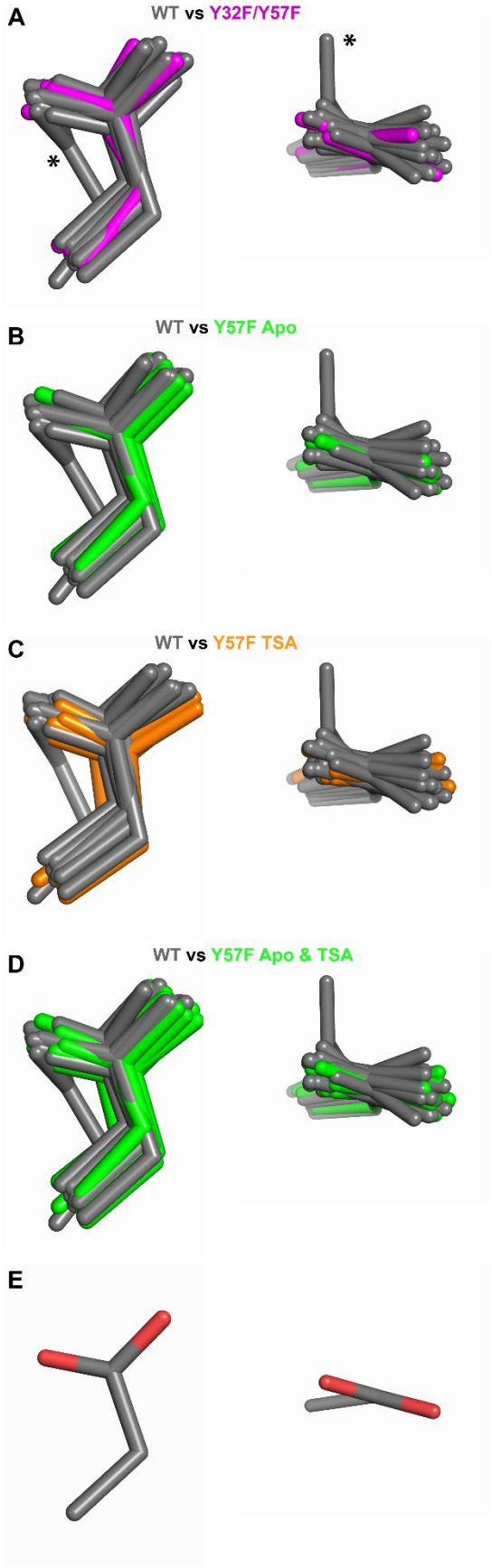

Figure S5. Comparison of WT and mutant general base D40 ensembles and multi-conformer models. Overlay of the WT ensemble (grey) with the multi-conformer models for (**A**) Y32F/Y57F (magenta), (**B**) Y57F apo, (**C**) Y57F TSA-bound (orange), and (**D**) Y57F apo and TSA-bound (green). For both WT and mutants, each KSI state is composed of the multi-conformer models for each monomer from the KSI dimer. Thus, the WT ensemble is composed of 2 multi-conformer models for each of the apo, GSA-bound, and TSA-bound states (*23*). For each mutant, each state is composed of two multi-conformer models. Thus the comparisons in (A-C) are between the WT ensemble and the two Y32F/Y57F apo multi-conformer models, the two Y57F apo multi-conformer models, and the two Y57F TSA-bound multi-conformer models, respectively. In (D) all four Y57F multi-conformer models (apo and TSA-bound) are compared with the WT ensemble. (**E**) Illustrates the orientation of general base D40 in (A-D) but with the oxygen atoms colored in red. The asterisk A denotes a general base "out" state that is observed in the complex of WT with bound ground state analog (PDB 6UCY, (*23*)). This seemingly rare "out" state is likely associated with the binding of ground state; its absence within mutant ensembles may be because it remains a rare state or may become less favored; nevertheless, it is not a reactive state and thus not expected to affect absolute or relative reaction rates.

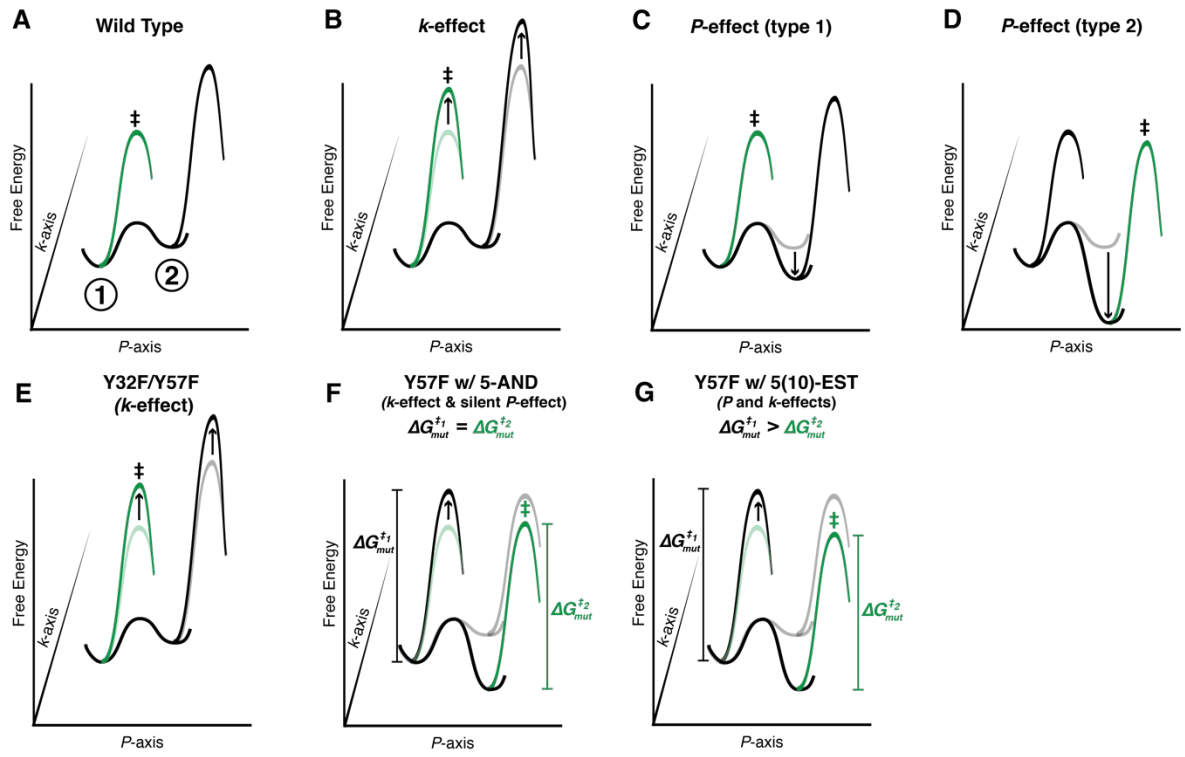

Figure S6. The effects of functional (*k*-effects) and occupancy changes (*P*-effects) to reactivity from an enzyme ensemble. In all panels, the *k*-axis is the reaction coordinate, the *P*-axis is the conformational coordinate, here simplified to two conformational states, and the Z-axis is free energy. Mutant profiles are in grey and light green, and the green profiles (with ≠) represent the preferred reaction path. Panels **A-D** reproduce Figure 6 from the main text. **A.** A simplified ensemble reaction coordinate for a WT enzyme that reacts preferentially from the most active and most probable state (green). A less reactive and less probable state is also depicted (black). **B.** Depiction of a *k*-effect, which increases the barrier to reaction uniformly in both states and reactions occur via the most populated state (≠, green). **C.** Depiction of a *P*-effect that changes the occupancy of states, but not the most reactive conformation. Reduced reactivity results from decreased occupancy of the more-reactive state. **D.** Depiction of a *P*-effect that results in the enzyme reacting from a more probable, but less reactive conformation (≠, green). **E.** The Y32F/Y57F KSI mutant displays a "*k*-effect" that decreases reaction rate by 4-fold in all conformers. **F.** The Y57F KSI mutant with the substrate 5-androstene-3,17-dione (5AND) displays a *k*-effect that decreases reaction rate by 9-fold in all conformers and a silent *P*-effect where the state probabilities change but this change is not responsible for the observed rate effect. **G.** The rate effect observed for the Y57F KSI mutant with the substrate 5(10)-estrene-3,17-dione (5(10)-EST) displays a combined *P*- and *k*-effect, where the increase in rate is mitigated by an *increase* in occupancy of a state that is better aligned for reaction with this substrate.

Supplementary Tables

RMSD (Å)	3VSY molecule B	1DMN	1DMM
3VSY molecule A	0.15	0.26	0.26
3VSY molecule B	-	0.25	0.25

Table S1. Alignment of WT (PDB 3VSY, (*35*)), Y32F/Y57F (PDB 1DMN, (*3*)), and Y57F (PDB 1DMM, (*3*)). The WT crystal structure contains two molecules (dimer) in the asymmetric unit, while Y32F/Y57F and Y57F asymmetric unit contains a single KSI molecule (monomer) and the KSI dimer can be reproduced by applying crystallographic two-fold symmetry. The KSI molecules are aligned on the protein backbone (atoms N, CA, C, O, see Materials and Methods).

Enzyme pKSI	k_{cat} (s^{-1})	K_M (μM)	k_{cat} rel	k_{cat} fold	K_M rel	Reference
Substrate 5-androstene-3,17-dione						
WT	21230 ± 80	49.9 ± 1.3	(1)	(1)	(1)	(*3*)
Y55F	3510 ± 60	23.0 ± 1.0	0.17	6.0	0.5	(*3*)
Y30F/Y55F	10680 ± 350	50.2 ± 5.5	0.50	2.0	1.0	(*3*)
WT	11000	81	(1)	(1)	(1)	(*33*)
Y57F	1193 ± 220	58 ± 26	0.11 ± 0.2	9.2 ± 1.7	0.7 ± 0.3	This work
Y32F/Y57F	2484 ± 271	23 ± 8	0.23 ± 0.2	4.4 ± 0.48	0.3 ± 0.1	This work
Substrate 5(10)-estrene-3,17-dione						
WT	9.9 ± 0.9	30 ± 4	(1)	(1)	(1)	(*33*)
Y57F	5.05 ± 0.5	30.2 ± 6.3	0.51 ± 0.1	2.0 ± 0.3	1.0 ± 0.25	This work
Y32F/Y57F	2.47 ± 0.3	21.9 ± 3.2	0.25 ± 0.3	4.0 ± 0.6	0.7 ± 0.14	This work
D40G	0.0021 ± 0.0001	30 ± 6	0.0002 ± 0.00002	4.7×10^3 ± 0.5×10^3	1.0 ± 0.24	(*72*)
Y57F/D40G	0.000152 ± 0.00003	54.2 ± 5.4	0.000015 ± 0.000003	65.1×10^3 ± 1.4×10^3	1.8 ± 0.30	This work
Y32F/Y57F/D40G	0.000412 ± 0.000016	25.5 ± 6.6	0.000042 ± 0.000004	24.0×10^3 ± 2.4×10^3	0.85 ± 0.25	This work
D40G	0.0021 ± 0.0001	30 ± 6	(1)	(1)	(1)	(*72*)
Y57F/D40G	0.000152 ± 0.00003	54.2 ± 5.4	0.07 ± 0.01	13.8 ± 2.3	0.6 ± 0.1	This work
Y32F/Y57F/D40G	0.000412 ± 0.000016	25.5 ± 6.6	0.20 ± 0.01	5.1 ± 0.3	1.2 ± 0.4	This work

Table S2. Enzyme kinetics data for KSI WT and mutants with two different substrates: 5-androstene-3,17-dione and 5(10)-estrene-3,17-dione (see Figure S4). The 5-androstene-3,17-dione kinetics data collected in (*33*) and in this work have been used for the analyses carried out. All K_M values are within two fold. Assuming that K_M approximates substrate affinity, the observed 2-fold effects suggest no changes in substrate affinity for any of the mutants.

	Y32F/Y57F apo	Y57F apo	Y57F TSA-bound
PDB code	7RXK	7RXF	7RY4
Data collection			
Wavelength (Å)	0.88557	0.88557	0.88557
Resolution range*	37.03-1.10 (1.12-1.10)	35.99-1.16 (1.18-1.16)	37.28-1.11 (1.13-1.11)
Space group	$P2_12_12_1$	$P2_12_12_1$	$P2_1$
Unit cell	36.27 74.06 96.23 90.00 90.00 90.00	35.99 74.14 95.64 90.00 90.00 90.00	36.24 74.55 50.97 90.00 110.70 90.00
Total reflections	687514 (31965)	580641 (26947)	371916 (17726)
Unique reflections	105295 (5087)	88770 (4193)	97398 (4738)
Multiplicity	6.5 (6.3)	6.5 (6.4)	3.8 (3.7)
Completeness (%)	99.4 (99.0)	99.5 (97.8)	97.8 (95.3)
Mean I/sigma(I)	9.2 (0.6)	7.7 (0.6)	7.4 (0.7)
R-merge	0.079 (2.860)	0.094 (2.851)	0.076 (1.764)
R-meas	0.086 (3.123)	0.102 (3.095)	0.088 (2.051)
R-pim	0.033 (1.233)	0.039 (1.192)	0.044 (1.028)
$CC_{1/2}$**	0.999 (0.315)	0.998 (0.435)	0.999 (0.303)
Refinement			
Resolution range	34.56-1.10 (1.14-1.10)	32.38-1.16 (1.20-1.16)	29.37-1.11 (1.15-1.11)
Reflections used in refinement*	104743 (10013)	88211 (8300)	97166 (9355)
Reflections used for R-free	5233 (472)	4393 (413)	4893 (498)
R-work	0.153 (0.337)	0.152 (0.337)	0.143 (0.300)
R-free	0.166 (0.324)	0.171 (0.342)	0.158 (0.300)
non-hydrogen atoms	5199	5241	6277
macromolecules	4870	4985	5850
ligands	6	4	130
solvent	323	252	297
Protein residues	257	254	257
RMS(bonds)	0.007	0.009	0.008
RMS(angles)	0.95	1.02	1.07
Ramachandran favored (%)	97.6	97.2	96.8
Ramachandran allowed (%)	2.4	2.8	3.2
Ramachandran outliers (%)	0.0	0.0	0.0
Average B-factor	17.8	19.9	14.5
macromolecules	17.0	19.3	13.8
ligands	17.0	21.5	16.6
solvent	29.4	31.6	27.1

*Values in parenthesis are for the highest resolution shells. ** $CC_{1/2}$ values are for the following resolution shells 7RXK: 1.10-1.13 Å, 7RXF: 1.16-1.19 Å, 7RY4: 1.11-1.14 Å.

Table S3. X-ray diffraction and model refinement statistic. All data collection statistics were obtained from Aimless (*77*, *78*), with the exception of $CC_{1/2}$, which was obtained from XSCALE from the XDS package (*76*). Model refinement statistics were obtained from phenix (*phenix.table_one*) using the final refined models and reflections files deposited on the PDB.

RMSD (Å)	WT Apo molA	WT Apo molB	Y32F/Y57F Apo molA	Y32F/Y57F Apo molB	Y57F Apo molA	Y57F Apo molB	Y57F TSA molA	Y57F TSA molB
WT Apo molA	-	0.31	0.25	0.45	0.35	0.40	0.39	0.41
WT Apo molB	0.31	-	0.35	0.35	0.41	0.42	0.42	0.40

Table S4. Alignment of multi-conformer models for WT and mutants. WT and mutant KSI crystals contain two molecules (dimer) in the asymmetric unit (molecule A and molecule B). RMSDs were calculated for each KSI molecule independently via alignment on the protein backbone (atoms N, CA, C, O, see Materials and Methods).

Enzyme	ΔHB length (Y16) Å	Reference
WT	(0)	(*50*)
Y32F	0.025	(*50*)
Y32F/Y57F	0.1	(*50*)
D103N	0.17	(*50*)
Y57F	0.14	This work

Table S5. Hydrogen bond length changes (ΔHB length) were obtained from ^{1}H solution NMR as previously described ((*50*, *52*) and see Materials and Methods).

Enzyme	$k_{cat, rel}$	k_{cat} rel	Log $k_{cat, rel}$	ΔHB length (Y16) Å
WT	11000	(1)	0	0
Y32F	-	-	-	0.025
Y32F/Y57F	2484	0.23	-0.64	0.1
Y57F	1193	0.11	-0.96	0.14
D103N	-	-	-	0.17

Table S6. Enzyme kinetics data for KSI WT and mutants with substrate 5-androstene-3,17-dione (from Table S2) and changes in hydrogen bond length (ΔHB length, from Table S5) used in Figures 2F and 3E.

Enzyme	k_{cat}	$k_{cat, rel}$	Log $k_{cat, rel}$	Enzyme	k_{cat}	$k_{cat, rel}$	Log k_{cat}, rel	ΔHB length (Y16) Å
WT	9.9	(1)	0	D40G	0.0021	(1)	0	0
Y32F	5	0.5	-0.3	Y32F/ D40G	-	-	-	0.025
Y32F/ Y57F	2.5	0.25	-0.6	Y32F/ Y57F/ D40G	0.00041	0.195	-0.71	0.1
Y57F	5.1	0.51	-0.29	Y57F/ D40G	0.000152	0.072	-1.14	0.14
D103N	0.76	0.077	-1.11	D103N/ D40G	-	-	-	0.17

Table S7. Enzyme kinetics data for KSI WT and mutants relative to WT (D40 background) or relative to D40G with substrate 5(10)-estrene-3,17-dione (from Table S2) and changes in hydrogen bond length (ΔHB length, from Table S5) used in Figures 2F and 3E.

REFERENCES AND NOTES

1. J. M. Berg, J. L. Tymoczko, L. Stryer, J. M. Berg, J. L. Tymoczko, L. Stryer, *Biochemistry* (W H Freeman, ed. 5, 2002).

2. A. Fersht, *Enzyme Structure and Mechanism* (W.H. Freeman, 1985).

3. D.-H. Kim, D. S. Jang, G. H. Nam, G. Choi, J.-S. Kim, N.-C. Ha, M.-S. Kim, B.-H. Oh, K. Y. Choi, Contribution of the hydrogen-bond network involving a tyrosine triad in the active site to the structure and function of a highly proficient ketosteroid isomerase from *Pseudomonas putida* biotype B. *Biochemistry* **39**, 4581–4589 (2000).

4. S. L. Lawson, W. W. Wakarchuk, S. G. Withers, Effects of both shortening and lengthening the active site nucleophile of bacillus circulans xylanase on catalytic activity. *Biochemistry* **35**, 10110–10118 (1996).

5. D. Straus, R. Raines, E. Kawashima, J. R. Knowles, W. Gilbert, Active site of triosephosphate isomerase: In vitro mutagenesis and characterization of an altered enzyme. *Proc. Natl. Acad. Sci. U.S.A.* **82**, 2272–2276 (1985).

6. I. V. Korendovych, W. F. DeGrado, Catalytic efficiency of designed catalytic proteins. *Curr. Opin. Struct. Biol.* **27**, 113–121 (2014).

7. V. Vaissier Welborn, T. Head-Gordon, Computational design of synthetic enzymes. *Chem. Rev.* **119**, 6613–6630 (2019).

8. T. Alber, W. A. Gilbert, D. R. Ponzi, G. A. Petsko, The role of mobility in the substrate binding and catalytic machinery of enzymes. *Ciba Found. Symp.* **93**, 4–24 (1983).

9. H. Frauenfelder, S. Sligar, P. Wolynes, The energy landscapes and motions of proteins. *Science* **254**, 1598–1603 (1991).

10. G. G. Hammes, S. J. Benkovic, S. Hammes-Schiffer, Flexibility, diversity, and cooperativity: Pillars of enzyme catalysis. *Biochemistry* **50**, 10422–10430 (2011).

11. J. P. Klinman, Dynamically achieved active site precision in enzyme catalysis. *Acc. Chem. Res.* **48**, 449–456 (2015).

12. R. Nussinov, C.-J. Tsai, H. Jang, Protein ensembles link genotype to phenotype. *PLOS Comput. Biol.* **15**, e1006648 (2019).

13. G. Wei, W. Xi, R. Nussinov, B. Ma, Protein ensembles: How does nature harness thermodynamic fluctuations for life? The diverse functional roles of conformational ensembles in the cell. *Chem. Rev.* **116**, 6516–6551 (2016).

14. R. B. Best, K. Lindorff-Larsen, M. A. DePristo, M. Vendruscolo, Relation between native ensembles and experimental structures of proteins. *Proc. Natl. Acad. Sci. U.S.A.* **103**, 10901–10906 (2006).

15. P. V. Burra, Y. Zhang, A. Godzik, B. Stec, Global distribution of conformational states derived from redundant models in the PDB points to non-uniqueness of the protein structure. *Proc. Natl. Acad. Sci. U.S.A.* **106**, 10505–10510 (2009).

16. V. Zoete, O. Michielin, M. Karplus, Relation between sequence and structure of HIV-1 protease inhibitor complexes: A model system for the analysis of protein flexibility. *J. Mol. Biol.* **315**, 21–52 (2002).

17. P. K. Agarwal, A biophysical perspective on enzyme catalysis. *Biochemistry* **58**, 438–449 (2019).

18. F. M. Menger, An alternative view of enzyme catalysis. *Pure Appl. Chem.* **77**, 1873–1886 (2005).

19. J. P. Klinman, S. Hammes-Schiffer, K. Arora, *Dynamics in Enzyme Catalysis* (Topics in Current Chemistry, Springer, 2013).

20. J. S. Fraser, M. W. Clarkson, S. C. Degnan, R. Erion, D. Kern, T. Alber, Hidden alternative structures of proline isomerase essential for catalysis. *Nature* **462**, 669–673 (2009).

21. R. B. Fenwick, H. van den Bedem, J. S. Fraser, P. E. Wright, Integrated description of protein dynamics from room-temperature x-ray crystallography and NMR. *Proc. Natl. Acad. Sci. U.S.A.* **111**, E445–E454 (2014).

22. D. D. Boehr, D. McElheny, H. J. Dyson, P. E. Wright, The dynamic energy landscape of dihydrofolate reductase catalysis. *Science* **313**, 1638–1642 (2006).

23. F. Yabukarski, J. T. Biel, M. M. Pinney, T. Doukov, A. S. Powers, J. S. Fraser, D. Herschlag, Assessment of enzyme active site positioning and tests of catalytic mechanisms through x-ray–derived conformational ensembles. *Proc. Natl. Acad. Sci. U.S.A.* **117**, 33204–33215 (2020).

24. H. van den Bedem, A. Dhanik, J.-C. Latombe, A. M. Deacon, Modeling discrete heterogeneity in x-ray diffraction data by fitting multi-conformers. *Acta Crystallogr. D Biol. Crystallogr.* **65**, 1107–1117 (2009).

25. D. A. Keedy, L. R. Kenner, M. Warkentin, R. A. Woldeyes, J. B. Hopkins, M. C. Thompson, A. S. Brewster, A. H. Van Benschoten, E. L. Baxter, M. Uervirojnangkoorn, S. E. McPhillips, J. Song, R. Alonso-Mori, J. M. Holton, W. I. Weis, A. T. Brunger, S. M. Soltis, H. Lemke, A. Gonzalez, N. K. Sauter, A. E. Cohen, H. van den Bedem, R. E. Thorne, J. S. Fraser, Mapping the conformational landscape of a dynamic enzyme by multitemperature and XFEL crystallography. *eLife* **4**, e07574 (2015).

26. J. S. Fraser, C. J. Jackson, Mining electron density for functionally relevant protein polysterism in crystal structures. *Cell. Mol. Life Sci.* **68**, 1829–1841 (2011).

27. D. A. Keedy, J. S. Fraser, H. van den Bedem, Exposing hidden alternative backbone conformations in x-ray crystallography using qFit. *PLoS Comput. Biol.* **11**, e1004507 (2015).

28. S. W. Kim, S.-S. Cha, H.-S. Cho, J.-S. Kim, N.-C. Ha, M.-J. Cho, S. Joo, K. K. Kim, K. Y. Choi, B.-H. Oh, High-resolution crystal structures of Δ5-3-ketosteroid isomerase with and without a reaction intermediate analogue. *Biochemistry* **36**, 14030–14036 (1997).

29. R. M. Pollack, Enzymatic mechanisms for catalysis of enolization: Ketosteroid isomerase. *Bioorg. Chem.* **32**, 341–353 (2004).

30. D. A. Kraut, P. A. Sigala, T. D. Fenn, D. Herschlag, Dissecting the paradoxical effects of hydrogen bond mutations in the ketosteroid isomerase oxyanion hole. *Proc. Natl. Acad. Sci. U.S.A.* **107**, 1960–1965 (2010).

31. A. Kuliopulos, A. S. Mildvan, D. Shortle, P. Talalay, Kinetic and ultraviolet spectroscopic studies of active-site mutants of. DELTA.5–3-ketosteroid isomerase. *Biochemistry* **28**, 149–159 (1989).

32. J. P. Schwans, P. Hanoian, B. J. Lengerich, F. Sunden, A. Gonzalez, Y. Tsai, S. Hammes-Schiffer, D. Herschlag, Experimental and computational mutagenesis to investigate the positioning of a general base within an enzyme active site. *Biochemistry* **53**, 2541–2555 (2014).

33. J. P. Schwans, F. Sunden, A. Gonzalez, Y. Tsai, D. Herschlag, Correction to "evaluating the catalytic contribution from the oxyanion hole in ketosteroid isomerase". *J. Am. Chem. Soc.* **138**, 7801–7802 (2016).

34. D. M. Blow, Rearrangement of Cruickshank's formulae for the diffraction-component precision index. *Acta Crystallogr. D Biol. Crystallogr.* **58**, 792–797 (2002).

35. N. Furnham, T. L. Blundell, M. A. DePristo, T. C. Terwilliger, Is one solution good enough? *Nat. Struct. Mol. Biol.* **13**, 184–185 (2006).

36. B. Halle, Biomolecular cryocrystallography: Structural changes during flash-cooling. *Proc. Natl. Acad. Sci. U.S.A.* **101**, 4793–4798 (2004).

37. D. H. Juers, B. W. Matthews, Reversible lattice repacking illustrates the temperature dependence of macromolecular interactions. *J. Mol. Biol.* **311**, 851–862 (2001).

38. D. A. Keedy, H. van den Bedem, D. A. Sivak, G. A. Petsko, D. Ringe, M. A. Wilson, J. S. Fraser, Crystal cryocooling distorts conformational heterogeneity in a model michaelis complex of DHFR. *Structure* **22**, 899–910 (2014).

39. A. Kuzmanic, N. S. Pannu, B. Zagrovic, X-ray refinement significantly underestimates the level of microscopic heterogeneity in biomolecular crystals. *Nat. Commun.* **5**, 3220 (2014).

40. Z. Sun, Q. Liu, G. Qu, Y. Feng, M. T. Reetz, Utility of B-factors in protein science: Interpreting rigidity, flexibility, and internal motion and engineering thermostability. *Chem. Rev.* **119**, 1626–1665 (2019).

41. D. A. Keedy, Z. B. Hill, J. T. Biel, E. Kang, T. J. Rettenmaier, J. Brandão-Neto, N. M. Pearce, F. von Delft, J. A. Wells, J. S. Fraser, An expanded allosteric network in PTP1B by multitemperature crystallography, fragment screening, and covalent tethering. *eLife* **7**, e36307 (2018).

42. D. Ringe, G. A. Petsko, The "glass transition" in protein dynamics: What it is, why it occurs, and how to exploit it. *Biophys. Chem.* **105**, 667–680 (2003).

43. R. F. Tilton, J. C. Dewan, G. A. Petsko, Effects of temperature on protein structure and dynamics: X-ray crystallographic studies of the protein ribonuclease-A at nine different temperatures from 98 to 320 K. *Biochemistry* **31**, 2469–2481 (1992).

44. M. M. Pinney, D. A. Mokhtari, E. Akiva, F. Yabukarski, D. M. Sanchez, R. Liang, T. Doukov, T. J. Martinez, P. C. Babbitt, D. Herschlag, Parallel molecular mechanisms for enzyme temperature adaptation. *Science* **371**, eaay2784 (2021).

45. D. Herschlag, M. M. Pinney, Hydrogen bonds: Simple after all? *Biochemistry* **57**, 3338–3352 (2018).

46. T. K. Harris, A. S. Mildvan, High-precision measurement of hydrogen bond lengths in proteins by nuclear magnetic resonance methods. *Proteins Struct. Funct. Genet.* **35**, 275–282 (1999).

47. G. A. Jeffrey, Y. Yeon, The correlation between hydrogen-bond lengths and proton chemical shifts in crystals. *Acta Crystallogr. B* **42**, 410–413 (1986).

48. A. S. Mildvan, T. K. Harris, C. Abeygunawardana, Nuclear magnetic resonance methods for the detection and study of low-barrier hydrogen bonds on enzymes. *Methods Enzymol.* **308**, 219–245 (1999).

49. M. M. Pinney, A. Natarajan, F. Yabukarski, D. M. Sanchez, F. Liu, R. Liang, T. Doukov, J. P. Schwans, T. J. Martinez, D. Herschlag, Structural coupling throughout the active site hydrogen bond networks of ketosteroid isomerase and photoactive yellow protein. *J. Am. Chem. Soc.* **140**, 9827–9843 (2018).

50. P. A. Sigala, J. M. M. Caaveiro, D. Ringe, G. A. Petsko, D. Herschlag, Hydrogen bond coupling in the ketosteroid isomerase active site. *Biochemistry* **48**, 6932–6939 (2009).

51. J. P. Schwans, D. A. Kraut, D. Herschlag, Determining the catalytic role of remote substrate binding interactions in ketosteroid isomerase. *Proc. Natl. Acad. Sci. U.S.A.* **106**, 14271–14275 (2009).

52. S. Shan, D. Herschlag, [11] Hydrogen bonding in enzymatic catalysis: Analysis of energetic contributions. *Methods Enzymol.* **308**, 246–276 (1999).

53. S. Shan, S. Loh, D. Herschlag, The energetics of hydrogen bonds in model systems: Implications for enzymatic catalysis. *Science* **272**, 97–101 (1996).

54. A. Broom, R. V. Rakotoharisoa, M. C. Thompson, N. Zarifi, E. Nguyen, N. Mukhametzhanov, L. Liu, J. S. Fraser, R. A. Chica, Ensemble-based enzyme design can recapitulate the effects of laboratory directed evolution in silico. *Nat. Commun.* **11**, 4808 (2020).

55. R. Otten, L. Liu, L. R. Kenner, M. W. Clarkson, D. Mavor, D. S. Tawfik, D. Kern, J. S. Fraser, Rescue of conformational dynamics in enzyme catalysis by directed evolution. *Nat. Commun.* **9**, 1314 (2018).

56. J. T. Biel, M. C. Thompson, C. N. Cunningham, J. E. Corn, J. S. Fraser, Flexibility and design: Conformational heterogeneity along the evolutionary trajectory of a redesigned ubiquitin. *Structure* **25**, 739–749.e3 (2017).

57. D. Petrović, V. A. Risso, S. C. L. Kamerlin, J. M. Sanchez-Ruiz, Conformational dynamics and enzyme evolution. *J. R. Soc. Interface* **15**, 20180330 (2018).

58. B. Ma, S. Kumar, C. J. Tsai, Z. Hu, R. Nussinov, Transition-state ensemble in enzyme catalysis: Possibility, reality, or necessity? *J. Theor. Biol.* **203**, 383–397 (2000).

59. H. G. Garcia, J. Kondev, N. Orme, J. A. Theriot, R. Phillips, A first exposure to statistical mechanics for life scientists. arXiv 0708.1899 [q-bio.QM] (14 August 2007).

60. K. Henzler-Wildman, D. Kern, Dynamic personalities of proteins. *Nature* **450**, 964–972 (2007).

61. P. K. Agarwal, N. Doucet, C. Chennubhotla, A. Ramanathan, C. Narayanan, Conformational sub-states and populations in enzyme catalysis. *Methods Enzymol.* **578**, 273–297 (2016).

62. A. R. Offenbacher, S. Hu, E. M. Poss, C. A. M. Carr, A. D. Scouras, D. M. Prigozhin, A. T. Iavarone, A. Palla, T. Alber, J. S. Fraser, J. P. Klinman, Hydrogen–Deuterium exchange of lipoxygenase uncovers a relationship between distal, solvent exposed protein motions and the thermal activation barrier for catalytic proton-coupled electron tunneling. *ACS Cent. Sci.* **3**, 570–579 (2017).

63. J. P. Klinman, A. Kohen, Hydrogen tunneling links protein dynamics to enzyme catalysis. *Annu. Rev. Biochem.* **82**, 471–496 (2013).

64. D. D. Boehr, R. Nussinov, P. E. Wright, The role of dynamic conformational ensembles in biomolecular recognition. *Nat. Chem. Biol.* **5**, 789–796 (2009).

65. H. N. Motlagh, J. O. Wrabl, J. Li, V. J. Hilser, The ensemble nature of allostery. *Nature* **508**, 331–339 (2014).

66. V. Lamba, F. Yabukarski, M. Pinney, D. Herschlag, Evaluation of the catalytic contribution from a positioned general base in ketosteroid isomerase. *J. Am. Chem. Soc.* **138**, 9902–9909 (2016).

67. D. A. Kraut, P. A. Sigala, B. Pybus, C. W. Liu, D. Ringe, G. A. Petsko, D. Herschlag, Testing electrostatic complementarity in enzyme catalysis: Hydrogen bonding in the ketosteroid isomerase oxyanion hole. *PLOS Biol.* **4**, e99 (2006).

68. D. L. Turner, Binomial solvent suppression. *J. Magn. Reson.* **54**, 146–148 (1983).

69. W. Doster, S. Cusack, W. Petry, Dynamical transition of myoglobin revealed by inelastic neutron scattering. *Nature* **337**, 754–756 (1989).

70. J. R. Lewandowski, M. E. Halse, M. Blackledge, L. Emsley, Protein dynamics. Direct observation of hierarchical Protein dynamics. *Science* **348**, 578–581 (2015).

71. W. Kabsch, XDS, *Acta Crystallogr. D Biol. Crystallogr.* **66**, 125–132 (2010).

72. Collaborative Computational Project, Number 4, The CCP4 suite: Programs for protein crystallography. *Acta Crystallogr. D Biol. Crystallogr.* **50**, 760–763 (1994).

73. P. R. Evans, G. N. Murshudov, How good are my data and what is the resolution? *Acta Crystallogr. D Biol. Crystallogr.* **69**, 1204–1214 (2013).

74. S. French, K. Wilson, On the treatment of negative intensity observations. *Acta Crystallogr. A* **34**, 517–525 (1978).

75. A. J. McCoy, R. W. Grosse-Kunstleve, P. D. Adams, M. D. Winn, L. C. Storoni, R. J. Read, Phaser crystallographic software. *J. Appl. Cryst.* **40**, 658–674 (2007).

76. G. Langer, S. X. Cohen, V. S. Lamzin, A. Perrakis, Automated macromolecular model building for x-ray crystallography using ARP/wARP version 7. *Nat. Protoc.* **3**, 1171–1179 (2008).

77. P. Emsley, K. Cowtan, Coot: Model-building tools for molecular graphics. *Acta Crystallogr. D Biol. Crystallogr.* **60**, 2126–2132 (2004).

78. P. V. Afonine, R. W. Grosse-Kunstleve, N. Echols, J. J. Headd, N. W. Moriarty, M. Mustyakimov, T. C. Terwilliger, A. Urzhumtsev, P. H. Zwart, P. D. Adams, Towards automated crystallographic structure refinement with phenix.refine. *Acta Crystallogr. D Biol. Crystallogr.* **68**, 352–367 (2012).

79. P. Emsley, B. Lohkamp, W. G. Scott, K. Cowtan, Features and development of Coot. *Acta Crystallogr. D Biol. Crystallogr.* **66**, 486–501 (2010).

80. V. B. Chen, W. B. Arendall, J. J. Headd, D. A. Keedy, R. M. Immormino, G. J. Kapral, L. W. Murray, J. S. Richardson, D. C. Richardson, MolProbity: All-atom structure validation for macromolecular crystallography. *Acta Crystallogr. D Biol. Crystallogr.* **66**, 12–21 (2010).

81. Schrödinger, The PyMOL Molecular Graphics System, Schrödinger, LLC.

82. D. W. J. Cruickshank, Remarks about protein structure precision. *Acta Crystallogr. D Biol. Crystallogr.* **55**, 583–601 (1999).

83. D. K. Kala Sekar, G. Manickam, S. N. Satheesh, P. Radha, S. Pavithra, K. Tharshan, J. Helliwell, Online-DPI: A web server to calculate the diffraction precision index for a protein structure. *J. Appl. Cryst.* **48**, 939–942 (2015).

84. D. Liebschner, M. Dauter, A. Brzuszkiewicz, Z. Dauter, On the reproducibility of protein crystal structures: Five atomic resolution structures of trypsin. *Acta Crystallogr. D Biol. Crystallogr.* **69**, 1447–1462 (2013).

85. F. Yabukarski, T. Doukov, D. A. Mokhtari, S. Du, D. Herschlag, Damaged goods? Evaluating the impact of x-ray damage on conformational heterogeneity in room temperature and cryo-cooled protein crystals. bioRxiv 2021.06.27.450091 [**Preprint**]. 28 June 2021. https://doi.org/10.1101/2021.06.27.450091.

86. W. W. Cleland, M. M. Kreevoy, Low-barrier hydrogen bonds and enzymic catalysis. *Science* **264**, 1887–1890 (1994).

87. J. A. Gerlt, M. M. Kreevoy, W. W. Cleland, P. A. Frey, Understanding enzymic catalysis: The importance of short, strong hydrogen bonds. *Chem. Biol.* **4**, 259–267 (1997).

88. J. D. Graham, A. M. Buytendyk, D. Wang, K. H. Bowen, K. D. Collins, Strong, low-barrier hydrogen bonds may be available to enzymes. *Biochemistry* **53**, 344–349 (2014).

89. I.-J. Lin, E. B. Gebel, T. E. Machonkin, W. M. Westler, J. L. Markley, Changes in hydrogen-bond strengths explain reduction potentials in 10 rubredoxin variants. *Proc. Natl. Acad. Sci. U.S.A.* **102**, 14581–14586 (2005).

90. T. Ishida, Low-barrier hydrogen bond hypothesis in the catalytic triad residue of serine proteases: Correlation between structural rearrangement and chemical shifts in the acylation process. *Biochemistry* **45**, 5413–5420 (2006).

91. J. P. Klinman, Low barrier hydrogen bonds: Getting close, but not sharing…. *ACS Cent. Sci.* **1**, 115–116 (2015).

92. C. L. Perrin, J. B. Nielson, "Strong" hydrogen bonds in chemistry and biology. *Annu. Rev. Phys. Chem.* **48**, 511–544 (1997).

93. S. Yamaguchi, H. Kamikubo, K. Kurihara, R. Kuroki, N. Niimura, N. Shimizu, Y. Yamazaki, M. Kataoka, Low-barrier hydrogen bond in photoactive yellow protein. *Proc. Natl. Acad. Sci. U.S.A.* **106**, 440–444 (2009).

94. A. Kobe, J. M. M. Caaveiro, S. Tashiro, D. Kajihara, M. Kikkawa, T. Mitani, K. Tsumoto, Incorporation of rapid thermodynamic data in fragment-based drug discovery. *J. Med. Chem.* **56**, 2155–2159 (2013).

95. I. P. Petrounia, R. M. Pollack, Substituent effects on the binding of phenols to the D38N mutant of 3-Oxo-Δ^5-steroid Isomerase.· A probe for the nature of hydrogen bonding to the intermediate. *Biochemistry* **37**, 700–705 (1998).

96. S. O. Shan, D. Herschlag, The change in hydrogen bond strength accompanying charge rearrangement: Implications for enzymatic catalysis. *Proc. Natl. Acad. Sci. U.S.A.* **93**, 14474–14479 (1996).

97. D. A. Mokhtari, M. J. Appel, P. M. Fordyce, D. Herschlag, High throughput and quantitative enzymology in the genomic era. *Curr. Opin. Struct. Biol.* **71**, 259–273 (2021).